# Photovoltaic Degradation Climate Zones

Todd Karin *, C. Birk Jones †, Anubhav Jain *

*Lawrence Berkeley National Laboratory, Berkeley, CA, U.S.A
†Sandia National Laboratory, Albuquerque, NM, U.S.A

***Abstract*—A large body of previous research indicates that climate affects photovoltaic (PV) degradation both in terms of steady power loss and hazardous failures. However, currently the geographic distribution of climate stressors has not been characterized in a systematic way. Most typically the Köppen-Geiger classification scheme is used for comparing PV degradation across different climates. However, Köppen-Geiger uses temperature and rainfall to develop zones relevant for botany and lacks the ability to distinguish locations based on climate stressors more relevant to PV degradation. Prior work has shown that specific stressors (e.g. high temperature, temperature cycling, damp heat, wind stress and UV exposure) induce multiple PV degradation modes such as solder bond degradation, corrosion by moisture intrusion, wind-induced cell cracking, encapsulant discoloration and others. We introduce a climate zone classification system specific to PV, PhotoVoltaic Climate Zones (PVCZ-2019 or PVCZ) that defines zones based on the geographic distribution in PV stressor intensity. This climate zone scheme provides quantitative thresholds on the climate stress experienced in each zone which can provide a basis for future work on the impact of climate on PV degradation and failure.**

***Index Terms*—photovoltaic, degradation, climate zones, Köppen Geiger, climate zone map, PVCZ**

## I. Introduction

SOLAR photovoltaic (PV) power generation investments benefit from an accurate long-term estimate of power and energy production. Often, PV analysts apply a loss factor of about 0.5 to 1% per year to account for an expected fall in power output caused by material degradation. However, previous studies have found that loss rates for individual systems vary from 0 to 2.5% per year depending on multiple factors including exposure to environmental stressors [1], [2]. An inaccuracy of 1.5% per year in linear degradation results in a 0.7 cents/kWh inaccuracy in total lifetime energy production out of a total system cost of 6-12 cents/kWh [3], making an $\sim$8% inaccuracy in levelized cost of electricity (LCOE). Along with increased maintenance costs and less-favorable financing terms due to this uncertainty, climate-induced degradation represents one of the larger unknowns when predicting LCOE [3].

In order to study how climate affects long-term photovoltaic performance and reliability, researchers have often used the Köppen-Geiger (KG) climate zone classification [4], [2]. KG defines climate zones based on seasonal precipitation and temperature patterns and was not created specifically for describing PV degradation, which makes studying the impact of climate on PV degradation difficult. This paper introduces a photovoltaic climate zone classification system (PVCZ-2019 or PVCZ for short) based on PV module degradation stressors specifically.

The specific stressors we use in our analysis are: Arrhenius-weighted mean module temperature, mean module temperature rate of change as a measure of thermal cycling, extreme low ambient temperature, wind stress, specific humidity as a measure of damp heat and UV exposure, which are identified in prior work [5], [6], [7], [8]. The PVCZ scheme can be used for future studies correlating observed degradation with climate, predicting the real-world longevity of a technology from indoor aging tests, making more precise LCOE calculations and engineering systems for resilience to climate stressors in the installation location.

## II. Weather data and climate stressors

Historical weather data is sourced from the Global Land Data Assimilation System (GLDAS) at 0.25 degree resolution across the world from Jan 1, 2010 to Dec 31, 2018 at 3 hour intervals [9], [10]. For quantifying temperature-related photovoltaic degradation, we use the module temperature, calculated as a temperature rise above ambient. This temperature rise depends on the details of the mounting configuration; typically roof-mounted systems have higher temperatures than open-rack mounted systems. Using King. et. al. as a model, module temperatures are calculated from ambient temperature, irradiance and wind speed using coefficients for open-rack polymer-back and close-roof-mount glass-back mounting configurations [11]. The array is assumed to be oriented in the same plane as the ground as this provides some balance between tracking and fixed-tilt systems in the estimated temperature. While these two temperature models cannot account for the continuous variety of different mounting configurations, they provide approximate limits on the expected dependence of mounting on temperature stress. This method predicts that two differently-mounted systems in the same location will experience different temperature stress, and therefore different degradation rates, consistent with field surveys.

Since the rate of many degradation processes such as solder bond degradation or encapsulant browning follows an Arrhenius dependence [13], [14], [15], an Arrhenius-weighted equivalent temperature $T_{\text{eq}}$ has been identified [6], [7] for quantifying the amount of temperature-activated stress present at each location, defined by

$$\exp\left(-\frac{E_a}{k_B T_{\text{eq}}}\right) = \frac{1}{t_2 - t_1}\int_{t_1}^{t_2} \exp\left(-\frac{E_a}{k_B T_m(t)}\right) dt \quad (1)$$

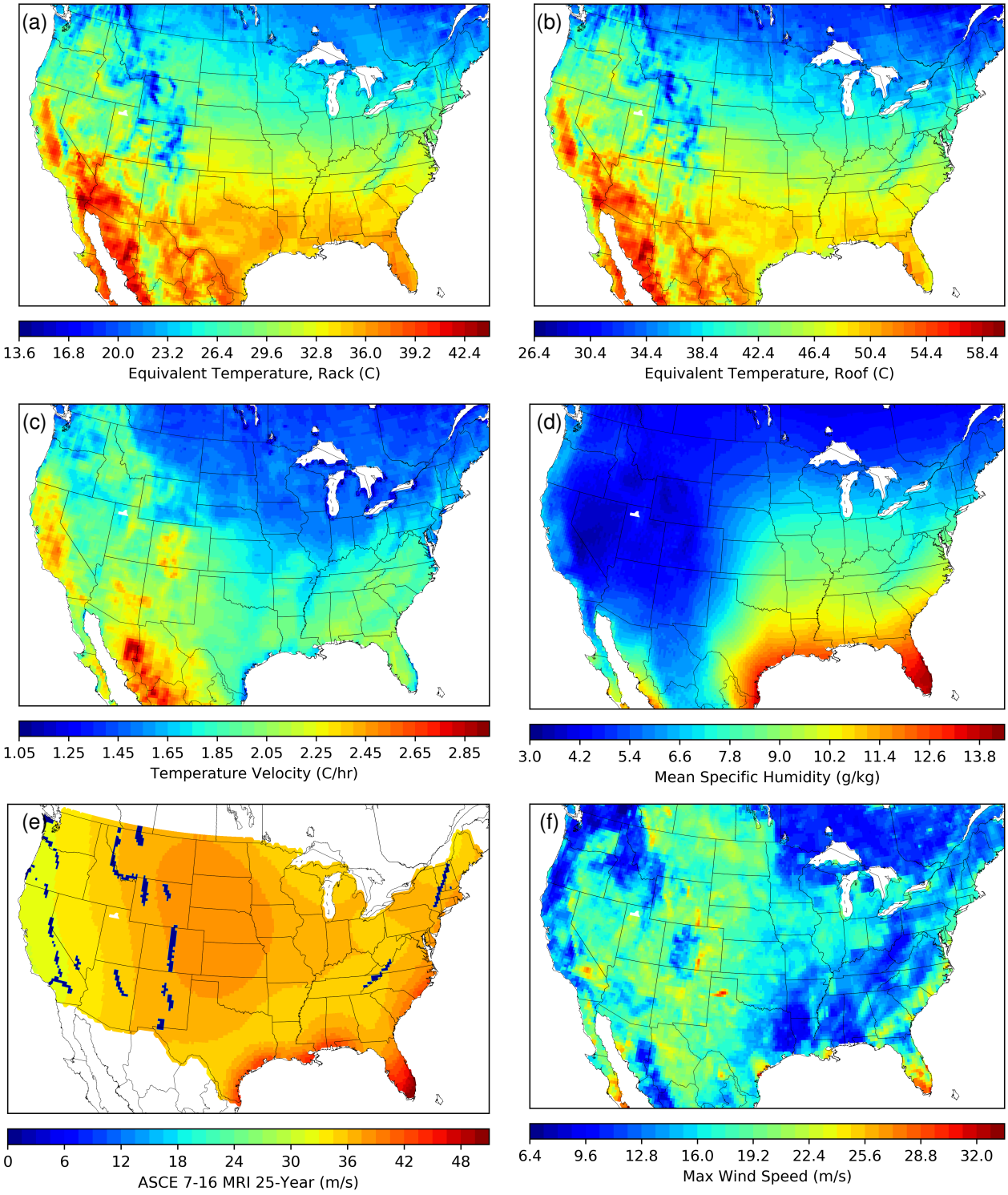


Fig. 1. Photovoltaic climate stressors. (a) Arrhenius weighted equivalent module temperature for open-rack mounted polymer back modules. (b) Mean rate of change of the equivalent module temperature. (c) Mean specific humidity. (d) American society of civil engineers 7-16 wind speed with a 25-year mean recurrence interval. Level 0 corresponds to a "special wind zone," an area where wind speeds are highly irregular due to local topography. (e) Global horizontal irradiance. (f) Max wind speed measured. Data for e is from ref. [12], all other data is from ref. [9], [10]

where $t_1$ and $t_2$ are the limits for the time integration, $E_a = 1.1$ eV is an activation energy, and $T_m(t)$ is the module temperature at time $t$. The choice of activation energy does change the temperature stress, but the stressor for a different activation energy, 0.55 eV, could be predicted within 2 C using a simple translation equation (data not shown). Therefore, even though the choice of activation energy is somewhat arbitrary, the geographic distribution of temperature stress is not very

sensitive to the choice of activation energy. The Arrhenius-weighted temperature is mainly responsive to time spent at elevated temperature: for example when equivalent time is spent at $50\,^{\circ}\mathrm{C}$ and $40\,^{\circ}\mathrm{C}$, $T_{\mathrm{eq}} = 46\,^{\circ}\mathrm{C}$, while for equivalent time at $50\,^{\circ}\mathrm{C}$ and $0\,^{\circ}\mathrm{C}$, $T_{\mathrm{eq}} = 44\,^{\circ}\mathrm{C}$. The distribution of equivalent temperature across the continental US (CONUS) is shown in Fig. 1(a)-(b) for open rack and roof mounted systems. Typically roof mounted systems have 10-15 C higher equivalent temperatures compared to open-rack mounted systems.

A single temperature cycle to temperatures lower than -30 C followed by repeated mechanical stress can lead to significant cell cracking [8]. We have calculated the minimum ambient temperature, which is well-correlated with the equivalent temperature distribution. This data is not shown for space constraints but is available in the provided dataset, see Sec. IV.

The mean module temperature rate of change

$$C = \frac{1}{t_2 - t_1} \int_{t_1}^{t_2} \left| \frac{dT_m}{dt} \right| dt, \tag{2}$$

is used as a measure of thermal cycling, providing a combined measure of the number and extent of the thermal cycles. Figure 1(c) shows the temperature cycling (using open-rack mount module temperatuer) is highest in California and the Southwest.

Accelerated lifetime tests often use a combination of high temperature and humidity to greatly increase degradation rates [16], [17]. As a measure of damp heat, we use the mean specific humidity:

$$H = \frac{1}{t_2 - t_1} \int_{t_1}^{t_2} \mathrm{SH}(t) dt, \tag{3}$$

where SH is the specific humidity, the mass of water divided by the mass of air. Since warm air can carry more moisture, the specific humidity provides a measure of damp heat. The specific humidity stress is highest in the South 1(d).

While typical temperature and humidity stresses are well-represented in GLDAS, wind is not. Extreme storms may only impact certain areas over the few years studied, making it difficult to predict the regions where extreme wind speeds would occur. In the US, the American Society of Civil Engineers (ASCE) has several standards that are used to choose the designed wind speed for buildings. We chose to use the ASCE 25-year mean-recurrence-interval (MRI) wind speed as a measure of wind stress, see Fig. 1(e). Since extreme winds only occur infrequently, this value gives the maximum 3-second gust wind speed that on average is observed once per 25 years. [Risk-Informed Mean Recurrence Intervals for Updated Wind Maps in ASCE 7-16]. During the period studied, from 2010 through 2018, hurricanes impacted the US, in Florida and Texas. These are visible in the max wind speed map, see Fig. 1(f). However, the max wind speed map does not fully capture the hurricane risk along the entire gulf coast. For this reason we have chosen to use the ASCE map. Future work could explore whether a longer analysis time for wind would result in a more accurate stress map.

## III. Photovoltaic Climate Zones

We develop the PVCZ-2019 scheme (referred to as PVCZ in this paper) by setting thresholds on individual climate stressors. In this threshold classification, each stressor is given a letter key and a number describing the stressor intensity in a particular location. For example, the classification T5:H2 corresponds to a location with an Arrhenius-weighted module temperature (T) at a stress level of 5 and a mean specific humidity level (H) of 2. Although two different module thermal models are developed, open-rack polymer-back (rack) and close-roof-mount glass-back (roof), in the following when we do not specify which temperature stress is used, we are referring to open-rack mount. The threshold limits of each zone are given in Table. I and shown graphically in Fig. 2 against the distribution of each stressor across the GLDAS domain.

The temperature zones can be further binned if necessary. For example, certain studies of photovoltaic degradation only find statistically significant results by binning temperature locations into “hot” and “not hot” locations [1], [2].

The thresholds for temperature, humidity and wind are defined by balancing multiple considerations. We first explored defining temperature thresholds by creating a distribution of systems at each location with temperatures ranging from roof to rack mounted, and defining the thresholds so that an equal land area falls into each bin. We then regularized the thresholds so that they are linearly spaced. For humidity, we used an “equal-area” approach: each zone contains the same number of points on the GLDAS land grid (cylindrically spaced). The wind speed zones are defined with respect to the ASCE 7-16 MRI 25-year data, with thresholds chosen to split the hurricane risk regions, tornado risk regions and lower risk areas. We have chosen to use 10 temperature zones and 5 humidity zones because this produces a reasonable number of combined temperature/humidity zones. Moreover, because of correlations between these two stressors, 99% of the earth’s land area is covered by just 28 combined temperature/humidity zones (if only open rack systems are considered). With these choices, the number of combined temperature/humidity zones is comparable to the KG classification scheme, which contains 30 different zones.

In order to limit the total number of zones, we consider the correlations between different stressor variables. Figure 3 shows the distribution of stressor intensity for each of the eight temperature zones for open-rack mounting. These plots demonstrate that equivalent temperature is well-correlated with temperature velocity, GHI, and min ambient temperature, but not with specific humidity. Therefore, to limit the number of zones in the PVSC scheme, we will use equivalent temperature, specific humidity and wind speed for classifying zones, noting that temperature velocity, GHI and minimum ambient temperature are correlated with equivalent temperature.

The individual zone maps for temperature, humidity and wind speed are shown in Fig. 4(a)-(d). The temperature zone map for CONUS shows most of the area falls into 4 different temperature zones. The humidity zones in Fig. 4(b) reflect the expected high damp-heat stress experienced in the South. The

TABLE I
Stressor thresholds for photovoltaic climate zones. Zone T2 comprises sites with module temperature between 14 and 19 C. Zone T1 comprises sites with module temperature lower than 14 C. Only 5 zones are defined for specific humidity and wind, a dash is used to signify "not applicable."

| | | Threshold | | | | | | | | |
|---|---|---|---|---|---|---|---|---|---|---|
| Description | Symbol | 1-2 | 2-3 | 3-4 | 4-5 | 5-6 | 6-7 | 7-8 | 8-9 | 9-10 |
| Module Temperature (°C) | T | 14 | 19 | 24 | 29 | 34 | 39 | 44 | 49 | 54 |
| Specific Humidity (g/kg) | H | 3.0 | 4.1 | 5.9 | 10.5 | - | - | - | - | - |
| Wind, 25-year MRI (m/s) | W | 1 | 33 | 36 | 39 | - | - | - | - | - |

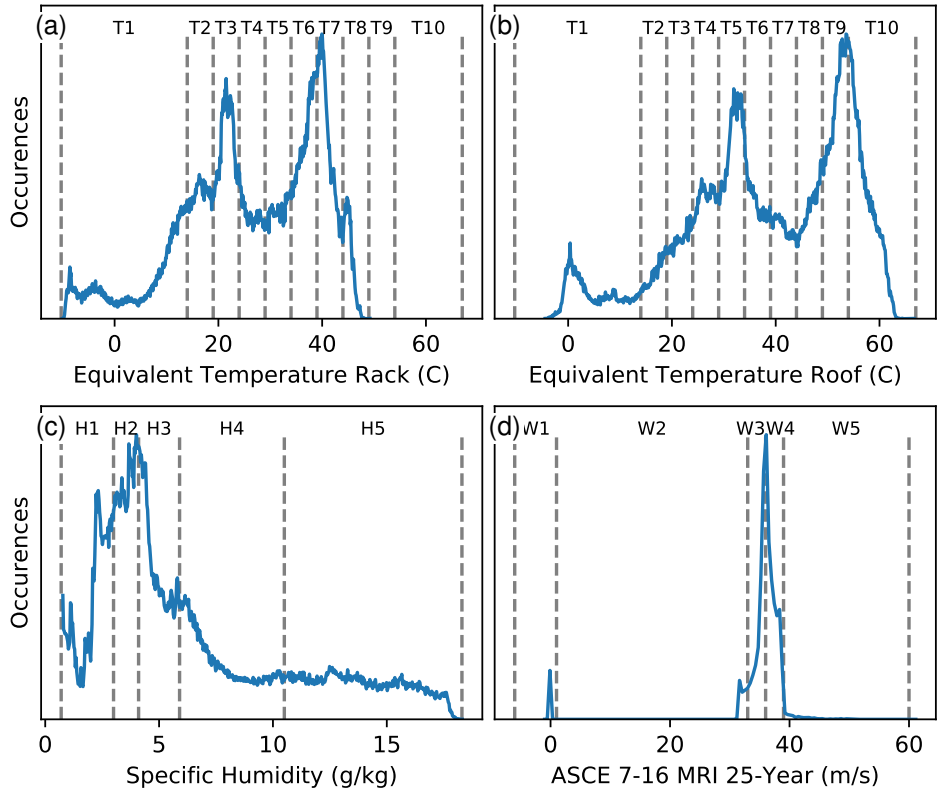


Fig. 2. Histograms of stressor variables, showing dividing lines for the definition of zones. (a) Using the open rack polymer-back temperature model, world land data points fall into eight different temperature zones. (b) Using a close-roof-mount temperature model, module temperatures are typically higher (c) Five humidity zones are defined with an "equal area" approach. (c) ASCE wind speed zone 1 includes "special wind zones."

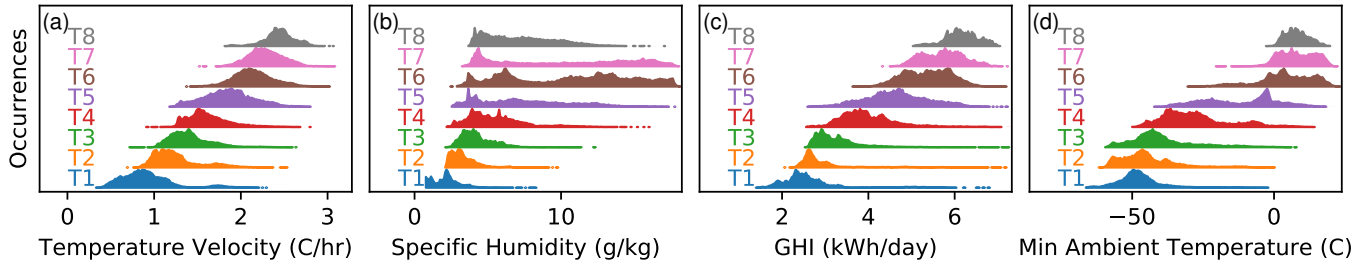


Fig. 3. (a) For each of the eight open-rack temperature zones, the distribution of module temperature velocity is shown. There is a strong correlation between temperature zone and temperature velocity. The histograms are normalized to the maximum value and shifted. (b) Mean specific humidity is not well correlated with temperature zone. For high temperature zones, there are dry locations (deserts) and humid locations (tropics). (c) Temperature zone is well correlated with GHI, which is proportional to UV stress. (d) Minimum ambient temperature is well correlated with equivalent temperature

wind speed zone map in Fig. 4(c) classifies the hurricane risk areas along the gulf coast in the highest wind zone W5. Much of the central part of the country falls into the second highest wind zone W4 due to high tornado risk.

The combined zone map in Fig. 4(d) shows the combination of temperature and humidity zones. These two stressors are highest in the South and lowest in the Rocky mountains and Nevada. The PV climate zone scheme can be compared with the KG temperature zones shown in Fig. 4(e) . We see that the KG temperature zone BSk extends from Mexico to Canada, whereas the PV temperature zone goes from T7 to T3 across this region. This is an example where a single KG zone

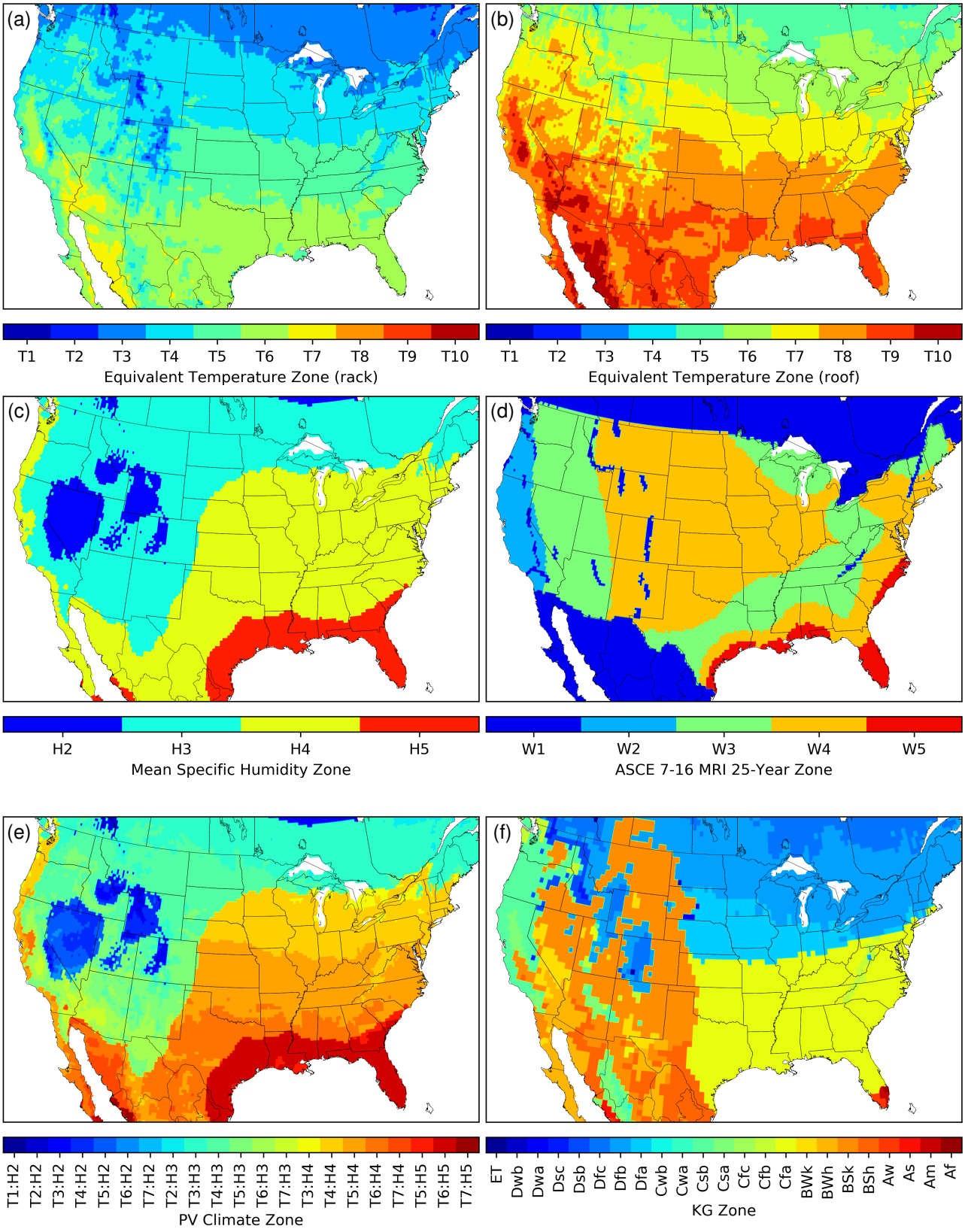


Fig. 4. Photovoltaic Climate Zones. (a) Temperature zones for CONUS (b) Specific Humidity zones. (c) Wind zones. (d) Combined temperature and humidity zones. Only those zones showing up in the plotted domain are listed in the colorbar. (e) KG temperature zones. (f). KG climate zones.

includes areas with a wide range of PV climate stressors. Lastly, the full KG zone map in Fig. 4(f) can be compared with the KG specific humidity zone map. KG is defined with respect to precipitation amounts and so does not properly

reflect the distribution in humidity, which is the more relevant PV stressor.

Prior to this analysis, it was not clear what the range of PV stress experienced in each KG zone. We show the distribution of PV stressors for each KG zone in Fig. 5(e)-(h), finding that in some KG zones (e.g. Af), there is a relatively tight distribution of stressors. However in other zones (e.g. BSk), a wider variety of PV stress is contained within a single KG zone. This is in contrast to the PV climate zone scheme where each zone contains well defined limits for temperature and humidity, see Fig. 5(a),(c). We note that both KG and PVCZ seem to have similar spread in the temperature velocity and GHI stressors, Fig. 5(b),(d).

In order to translate prior work performed with the KG classification into the relevant results with PVCZ, we have made the lookup tables for showing the most likely PVCZ zone for each KG zone. Figure. 6 shows a 2D histogram of what fraction of global land data points fall into each combined KG and PVCZ zone. A red square outlines the most likely choice of PVCZ zone for each KG zone.

## IV. Description of Dataset

The climate stressors and zones are provided as an open-access csv file on the DuraMAT datahub: https://datahub.duramat.org/dataset/pvcz. In the future, a python library will be provided for easy access to this dataset at the following location: https://github.com/toddkarin/pvcz.

A description of the variables included in the csv file are as follows:

- `lat`: latitude in fractional degrees.
- `lon`: longitude in fractional degres.
- `T_equiv_rack`: Arrhenius-weighted module equivalent temperature calculated using open-rack polymer-back temperature model and activation energy 1.1 eV, in C
- `T_equiv_roof`: Arrhenius-weighted module equivalent temperature calculated using close-roof-mount glass-back temperature model and activation energy 1.1 eV, in C
- `specific_humidity_mean`: Average specific humidity, in g/kg.
- `T_velocity`: Average rate of change of module temperature using open-rack polymer-back temperature model, in C/hr.
- `GHI_mean`: Mean global horizontal irradiance, in kWh/m$^2$/day.
- `wind_speed`: ASCE wind speed with a mean recurrence interval of 25 years, in m/s.
- `T_ambient_min`: Minimum ambient temperature, in C
- `KG_zone`: Köppen Geiger zone.
- `T_equiv_rack_zone`: Temperature zone for open-rack modules as a number 0 through 9, equivalent to temperature zones T1 through T10 respectively.
- `T_equiv_roof_zone`: Temperature zone for close-roof-mount modules as a number 0 through 9, equivalent to temperature zones T1 through T10 respectively.
- `specific_humidity_mean_zone`: Specific humidity zone, as a number 0 through 4, equivalent to temperature zones H1 through H5 respectively.
- `wind_speed_zone`: Wind speed zone as a number 0 through 4, equivalent to wind zones W1 through W5 respectively.
- `pvcz`: Combined temperature (rack) and humidity zones as a number 0 through 49, corresponding to temperature zones T1:H1, T2:H1, ... , T10:H5.
- `pvcz_labeled`: Combined temperature (rack) and humidity zones as an alpha-numeric key, e.g. T5:H2.

## V. Conclusion and Outlook

We have developed a climate zone scheme specific to degradation stressors affecting PV. The PVCZ scheme allows a detailed understanding of which types of degradation may be expected in different geographic areas. Future work can utilize the developed climate classification scheme to study the effects of climate stressors on the prevalence of specific degradation modes and the overall power degradation rate $R_D$.

The zone scheme can also be used for system engineering and financing. With a more detailed understanding of the extent of degradation expected for a particular site, the system design and financial models can be adjusted accordingly, resulting more precise system optimization and more accurate production estimates.

## Acknowledgment

This material is based upon work supported by the U.S. Department of Energy's Office of Energy Efficiency (DOE) and Renewable Energy (EERE) under Solar Energy Technologies Office (SETO) Agreement Number DE-EE0007137. Lawrence Berkeley National Laboratory is funded by the DOE under award DE-AC02-05CH11231. Sandia National Laboratories is a multimission laboratory managed and operated by National Technology and Engineering Solutions of Sandia, LLC., a wholly owned subsidiary of Honeywell International, Inc., for the U.S. DOE's National Nuclear Security Administration under contract DE-NA0003525.

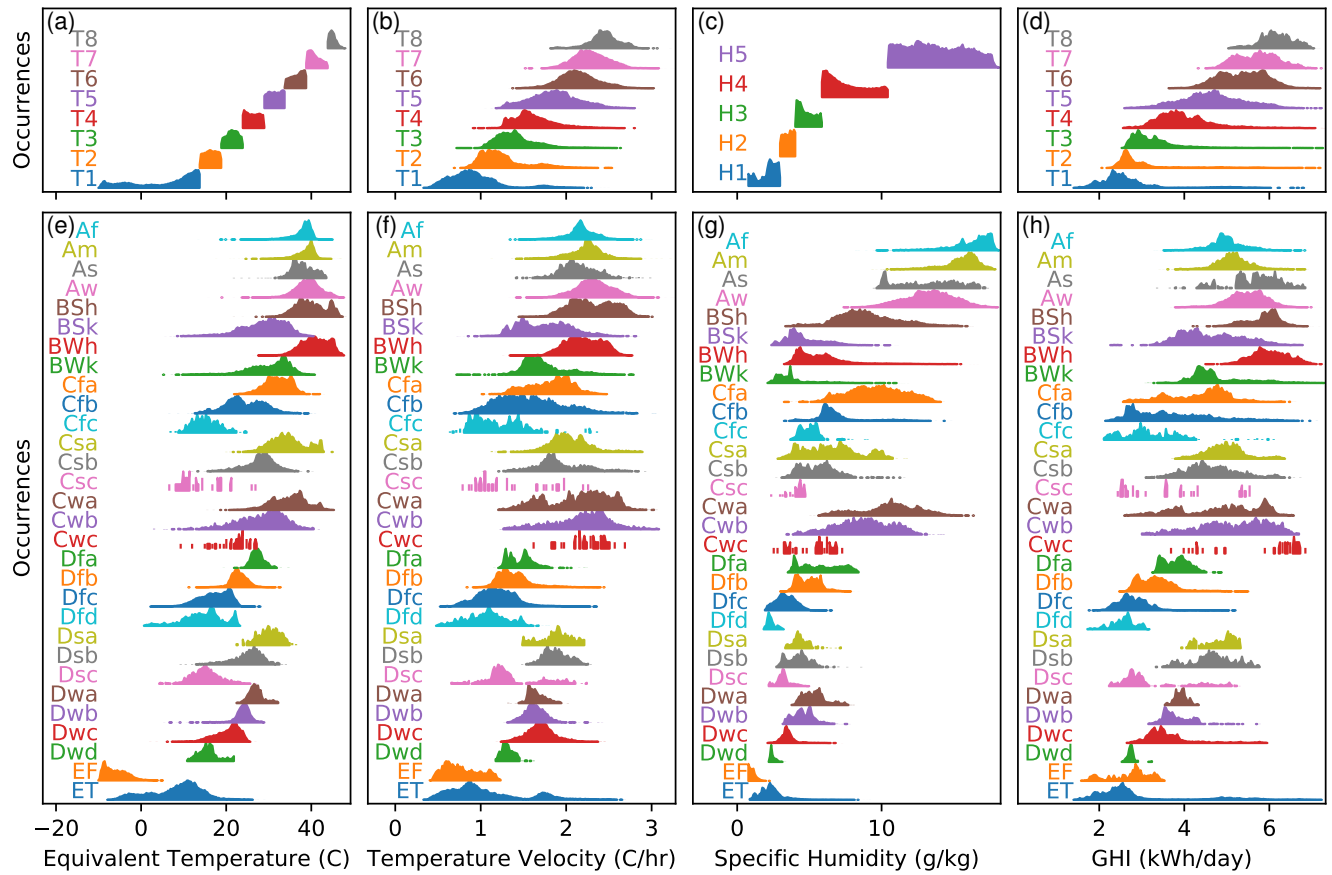


Fig. 5. Comparison of the stressor spread using KG and PVCZ. (a) Each temperature zone has strict limits for the distribution of equivalent temperature. (b) Each temperature zone shows a distribution of temperature velocity stress. (c) PVCZ is defined with respect to five specific humidity zones. (d) Each temperature zone has a range of GHI. (e) For each KG zone, the distribution of equivalent temperature is shown. Some KG zones show a wide distribution of equivalent temperature which covers multiple PVCZ temperature zones. (f) Distribution of temperature velocity for each KG zone. (g) Distribution of specific humidity stress for each KG zone. (h) Distribution of GHI for each KG zone.

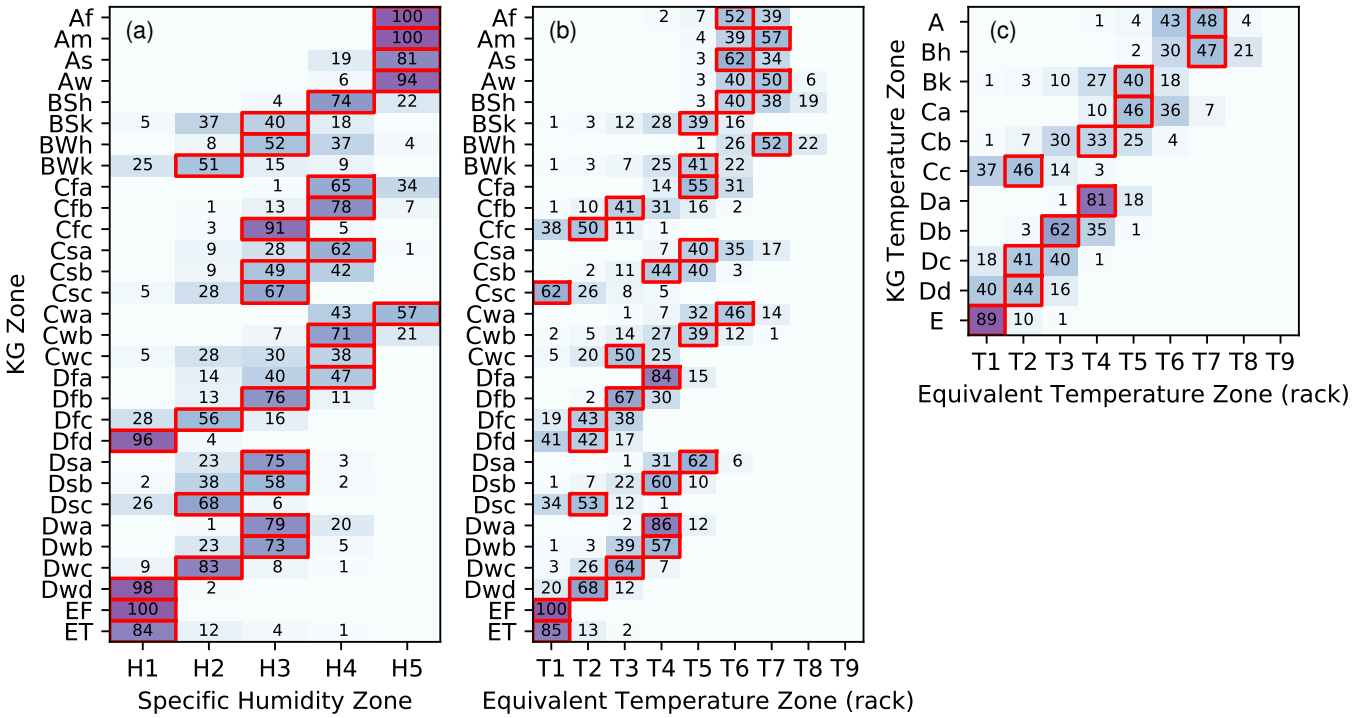


Fig. 6. Table showing the most likely PVCZ zone for each KG zone. For example, for the KG zone BSk, the greatest number of points fall into PVCZ zone H3 and T5.

## REFERENCES


[1] D. C. Jordan, S. R. Kurtz, K. VanSant, and J. Newmiller, "Compendium of photovoltaic degradation rates," *Progress in Photovoltaics: Research and Applications*, vol. 24, no. 7, pp. 978–989, 2016. [Online]. Available: https://onlinelibrary.wiley.com/doi/abs/10.1002/pip.2744

[2] S. Chattopadhyay, R. Dubey, V. Kuthanazhi, S. Zachariah, S. Bhaduri, C. Mahapatra, S. Rambabu, F. Ansari, A. Chindarkar, A. Sinha, H. K. Singh, N. Shiradkar, B. M. Arora, A. Kottantharayil, K. L. Narasimhan, A. Sabnis, J. Vasi, B. Bora, G. Kumar, Y. K. Singh, M. Bangar, M. Kumar, A. K. Haldkar, R. Singh, S. Raghava, M. Morampudi, G. Ganesh, R. Kumar, and O. S. Sastry, "All-india survey of photovoltaic module reliability: 2016," National Centre for Photovoltaic Research and Education (NCPRE), IIT Bombay and National Institute of Solar Energy (NISE), Gurugram, Tech. Rep., March 2017. [Online]. Available: http://www.ncpre.iitb.ac.in/research/pdf/All_India_Survey_of_Photovoltaic_Module_Reliability_2016.pdf

[3] R. Jones-Albertus, D. Feldman, R. Fu, K. Horowitz, and M. Woodhouse, "Technology advances needed for photovoltaics to achieve widespread grid price parity," *Progress in Photovoltaics: Research and Applications*, vol. 24, no. 9, pp. 1272–1283, 2016. [Online]. Available: https://onlinelibrary.wiley.com/doi/abs/10.1002/pip.2755

[4] W. Köppen, "Classification of climates according to temperature, precipitation and seasonal cycle," *Petermanns Geogr. Mitt*, vol. 64, pp. 193–203, 1918.

[5] C. B. Jones, T. Karin, and A. Jain, "Geographic assessment of photovoltaic module environmental degradation stressors," in *Photovoltaics Specialist Conference*, 2019.

[6] M. D. Kempe and J. H. Wohlgemuth, "Evaluation of temperature and humidity on pv module component degradation," in *2013 IEEE 39th Photovoltaic Specialists Conference (PVSC)*, June 2013, pp. 0120–0125.

[7] P. Mundle, N. Shiradkar, J. Vasi, and S. Patwardhan, "Photovoltaic climate classification for the degradation study," in *EUPVSC*, 2018.

[8] H. Seigneur, E. Schneller, J. Lincoln, A. Gabor, M. Rowell, H. Ebrahimi, R. Ghosh, and V. Huayamave, "Microcrack formation in silicon solar cells during cold temperatures," in *Photovoltaic Specialist Converence*, 2019.

[9] H. Beaudoing and M. Rodell, "Gldas noah land surface model l4 3 hourly 0.25 x 0.25 degree v2.1," *Goddard Earth Sciences Data and Information Services Center (GES DISC),*, p. 10.5067/E7TYRXPJKWOQ, 2016.

[10] M. Rodell, P. Houser, U. Jambor, J. Gottschalck, K. Mitchell, C. Meng, K. Arsenault, B. Cosgrove, J. Radakovich, M. Bosilovich, J. Entin, J. Walker, D. Lohmann, , and D. Toll, "The global land data assimilation system," *Bull. Amer. Meteor. Soc.*, vol. 85, p. 381, 2004.

[11] D. King, W. Boyson, and J. Kratochvill, "Photovoltaic array performance model," *SAND2004-3535*, 2004.

[12] A. S. of Civil Engineers, *Minimum Design Loads and Associated Criteria for Buildings and Other Structures*. American Society of Civil Engineers, 2017.

[13] G. Z. Wang, Z. N. Cheng, K. Becker, and J. Wilde, "Applying anand model to represent the viscoplastic deformation behavior of solder alloys," *Journal of Electronic Packaging*, vol. 123, no. 3, pp. 247–253, 10 1998. [Online]. Available: http://dx.doi.org/10.1115/1.1371781

[14] D. J. V. Kumar, "Determination of activation energy for encapsulant browning of photovoltaic modules," Master's thesis, ARIZONA STATE UNIVERSITY, 2016.

[15] A. Ndiaye, A. Charki, A. Kobi, C. M. Kébé, P. A. Ndiaye, and V. Sambou, "Degradations of silicon photovoltaic modules: A literature review," *Solar Energy*, vol. 96, pp. 140 – 151, 2013. [Online]. Available: http://www.sciencedirect.com/science/article/pii/S0038092X13002703

[16] P. Hacke, M. Kempe, K. Terwilliger, S. Glick, N. Call, S. Johnston, and S. Kurtz, "Characterization of multicrystalline silicon modules with system bias voltage applied in damp heat," *25th European Photovoltaic Solar Energy Conference and Exhibition*, 7 2010.

[17] C. Peike, S. Hoffmann, P. Hulsmann, B. Thaidigsmann, K. Weib, M. Koehl, and P. Bentz, "Origin of damp-heat induced cell degradation," *Solar Energy Materials and Solar Cells*, vol. 116, pp. 49 – 54, 2013. [Online]. Available: http://www.sciencedirect.com/science/article/pii/S0927024813001359